Secondary Structure and Lipid Interactions of the N-Terminal Segment of Pulmonary Surfactant SP-C in Langmuir Films: IR Reflection−Absorption Spectroscopy and Surface Pressure Studies[†]

Xiaohong Bi,[‡] Carol R. Flach,[‡] Jesus Pérez-Gil,[§] Inés Plasencia,[§] David Andreu,[||] Eliandre Oliveira,[||] and Richard Mendelsohn*,[‡]

Department of Chemistry, Newark College of Arts and Science, Rutgers University, 73 Warren Street, Newark, New Jersey 07102, Departamento de Bioquímica, Facultad de Biología, Universidad Complutense, 28040 Madrid, Spain, and Departamento Ciències Experimentals i de la Salut, Universidad Pompeu Fabra, 08003 Barcelona, Spain

Received February 13, 2002

ABSTRACT: Pulmonary surfactant, a thin lipid/protein film lining mammalian lungs, functions in vivo to reduce the work of breathing and to prevent alveolar collapse. Analogues of two hydrophobic surfactant proteins, SP-B and SP-C, have been incorporated into therapeutic agents for respiratory distress syndrome, a pathological condition resulting from deficiency in surfactant. To facilitate rational design of therapeutic agents, a molecular level understanding of lipid interaction with surfactant proteins or their analogues in aqueous monolayer films is necessary. The current work uses infrared reflection−absorption spectroscopy (IRRAS) to determine peptide conformation and the effects of S-palmitoylation on the lipid interactions of a synthetic 13 residue N-terminal peptide [SP-C13(palm)$_2$] of SP-C, in mixtures with 1,2-dipalmitoylphosphatidylcholine (DPPC) or 1,2-dipalmitoylphosphatidylglycerol (DPPG). Two Amide I′ features, at ∼1655 and ∼1639 cm^{-1} in the peptide IRRAS spectra, are assigned to α-helical peptide bonds in hydrophobic and aqueous environments, respectively. In binary DPPC/SP-C13(palm)$_2$ films, the proportion of hydrated/hydrophobic helix increases reversibly with surface pressure (π), suggestive of the peptide being squeezed out from hydrophobic regions of the monolayer. No such effect was observed for DPPG/peptide monolayers, indicative of stronger, probably electrostatic, interactions. Depalmitoylation produced a weakened interaction with either phospholipid as deduced from IRRAS spectra and from π−area isotherms. S-Palmitoylation may modulate peptide hydration and conformation in the N-terminal region of SP-C and may thus permit the peptide to remain in the film at the high surface pressures present during lung compression. The unique capability of IRRAS to detect the surface pressure dependence of protein or peptide structure/interactions in a physiologically relevant model for surfactant is clearly demonstrated.

Pulmonary surfactant, a lipid/protein mixture secreted from type II cells in the mammalian lung, functions in vivo to reduce surface tension at the air/alveolar interface, thereby facilitating the work of breathing and preventing alveolar collapse. Four surfactant-specific proteins (SP-A, SP-B, SP-C, and SP-D) have been identified. Of these, SP-A is a multimeric, water-soluble, Ca^{2+}-dependent collagenous lectin implicated in a variety of functions including surfactant homeostasis, biophysical activity, and host-defense. SP-D possesses structural elements similar to SP-A, although its function is unclear. SP-B and SP-C are small hydrophobic proteins processed from large precursors which enhance the rate of adsorption of phospholipids from the subphase to the air/water interface and facilitate spreading across the interface. For recent reviews on surfactant properties, refer to (*1*−*3*). These properties have led to the development of therapeutic agents for respiratory distress syndrome, a condition resulting from deficiency in surfactant. In premature infants, treatments for this condition, using preparations in which SP-B and/or SP-C are reconstituted with one or more of the pulmonary surfactant phospholipids, have had mixed clinical success.

The possible utility of SP-B and SP-C for therapeutic intervention has resulted in a plethora of studies aimed at elucidating structure−function relationships for these molecules. A variety of biophysical approaches have been employed to study either the intact proteins or synthetic fragments. The overall aim of such investigations is to provide a framework for the rational design of therapeutic agents (*4*, *5*).

An important element of SP-C structure results from posttranslational covalent modification. The polypeptide chain is converted into a lipoprotein at residues Cys-5 and Cys-6 which are palmitoylated via thioester linkages. The primary structure of this small, 4.2 kDa acylated polypeptide reveals a stretch of highly hydrophobic residues (porcine

[†] This work was supported by USPHS Grant GM 29864 (R.M.) and DGESIC, Spain, Grant BIO2000-0292 (J.P.-G.).

* To whom correspondence should be addressed. Phone: (973) 353-5613. Fax: (973) 353-1264. E-Mail: mendelso@andromeda.rutgers.edu.

[‡] Newark College of Arts and Science, Rutgers University.

[§] Universidad Complutense.

[||] Universidad Pompeu Fabra.

10.1021/bi020129g CCC: $22.00
Published on Web 06/04/2002

variant: LRIPCCPVNLKRLLVVVVVVVLVVVVIVGALLMGL). The structure of native SP-C in organic solvents determined by the Wuthrich group (*6*) reveals a very regular α-helical structure from residues 9−34, with a flexible disordered N-terminal segment. Several studies have examined the consequences of SP-C palmitoylation. In a general way, the molecular origin of any effects of S-palmitoylation presumably lies in the hydrophobicity of the chains, which would be expected to enhance the interaction of the protein with lipid films. This form of protein acylation is thought to anchor soluble proteins to membranes. Creuwels et al. (*7*) showed that S-palmitoylation of SP-C altered the $CaCl_2$-induced insertion of small unilamellar vesicles into preformed lipid/SP-C monolayers. In addition, Wang et al. (*8*) observed a significantly reduced rate of readsorption and decreased film stability for deacylated calf SP-C under rapid recycling conditions, thought to be analogous to processes in vivo. In an attempt to determine the molecular basis of these effects, this laboratory showed that deacylation of SP-C produces more fluid, expanded monolayers of DPPC[1] at pressures less than 30 mN/m, while the helical secondary structure of the peptide and tilt angle (∼70° relative to the surface normal) in monolayer films remained essentially unchanged upon deacylation (*9, 10*). CD studies comparing acylated and deacylated SP-C in lipid micelles demonstrated that although both are predominantly helical, the amount of α-helix decreased by ∼20% for the deacylated peptide (*11*).

The role of the N-terminal sequence in SP-C has not been widely studied, and the effects of S-palmitoylation on the properties of the N-terminus have not yet been determined. A few physical studies have begun to address these issues. In one study, a dansylated form of porcine SP-C indicated that the N-terminus of the protein was located near the surface of lipid bilayers and was exposed to the aqueous environment (*12*). Investigations using peptide fragments based on the N-terminal sequence of SP-C have also been conducted. Plasencia et al. (*13*) examined nonpalmitoylated synthetic peptides consisting of the 13 N-terminal residues using fluorescence and surface pressure−molecular area (π−*A*) isotherms to explore lipid interactions in bilayers and monolayers. CD spectroscopy was also used to evaluate peptide conformation in solution and lipid micelles. A mix of helical and unordered structures were reported, which is consistent with earlier NMR and CD studies of a nonpalmitoylated 17 residue peptide in micelle-bound form (*14*). A subsequent publication reported that palmitoylation of the 17 residue peptide increased the amount of helix present (*15*).

The current work extends prior studies and focuses on the structure and lipid interactions of a synthetic, S-palmitoylated, 13 residue peptide based on the N-terminal sequence of porcine SP-C, SP-C13$(palm)_2$, in phospholipid monolayers. The two phospholipids used in the studies, 1,2-dipalmitoylphosphatidylcholine (DPPC) and 1,2-dipalmitoylphosphatidylglycerol (DPPG), represent the major lipid classes in pulmonary surfactant. To directly monitor the effect of S-palmitoylation on the lipid/peptide interaction, the results for SP-C13$(palm)_2$ are compared with a deacylated L1W derivative of the peptide (SP-$C13_{L1W}$). The L→W substitution at position 1 was utilized in prior bulk phase fluorescence measurements. As a control, experiments were also conducted using a palmitoylated version of the L1W peptide, SP-$C13_{L1W}(palm)_2$.

To acquire molecular information about protein secondary structure and lipid acyl chain conformational order directly from the lipid and protein constituents of monolayer films at the air/water interface, the techniques of infrared reflection−absorption spectroscopy (IRRAS) are utilized in the current work. This approach was originated in the mid 1980s by Dluhy and co-workers, who demonstrated the feasibility of acquiring IR spectra from aqueous Langmuir films of fatty acids and phospholipids in situ at the air/water interface (*16, 17*). With the success of these measurements, IRRAS provided the means to monitor lipid conformational order and phase behavior. A variety of biologically motivated extensions of this technology ensued. This laboratory and the Bordeaux group independently developed methods for the acquisition of protein or peptide secondary structure information from monolayer films in the presence and absence of lipids. The Rutgers group implemented a sample shuttle approach in which interference from water vapor in the 1500−1800 cm^{-1} region where protein Amide I and II modes absorb was substantially reduced (*18*). This approach is used in the current study. Similar gains were achieved by the Bordeaux group through a polarization modulation experiment (PM-IRRAS) in which the polarization of the incident electric field is rapidly modulated between the s- and p-channels (*19*).

EXPERIMENTAL PROCEDURES

Materials. DPPC and DPPG were purchased from Avanti Polar Lipids (Alabaster, AL). Chloroform, methanol, EDTA, and HPLC-grade water were obtained from Fisher Scientific (Pittsburgh, PA). Trizma [tris(hydroxymethyl)aminomethane] hydrochloride and sodium chloride were purchased from Sigma (St. Louis, MO). D_2O with 99.9% isotopic enrichment was purchased from Cambridge Isotope Laboratories (Andover, MA).

Peptide Synthesis, Acylation, and Purification. Solid-phase synthesis of the peptide SP-$C13_{L1W}$ was done manually using BOC chemistry protocols on a *p*-methylbenzhydrylamine resin (0.45 mmol/g) at a 0.1 mmol scale, according to the method of Merrifield (*20*) as previously described (*21*). The palmitoylated peptides were synthesized by a solid-phase procedure adapted from Beekman et al. (*22*), with modifications. The sequences were assembled by Fmoc chemistry protocols on a poly(ethylene glycol)-polystyrene resin (*23*) functionalized with the 2,4-dimethoxy-4′-(carboxymethyloxy)benzhydrylamine handle. The cysteine side chains were originally protected with acetamidomethyl groups. After chain assembly, the acetamidomethyl groups were selectively released from the peptide resin by treatment with 0.1 M mercuric acetate in dimethyl formamide (DMF) for 3 h; the peptide resin was treated with 10% (by volume) 2-mercaptoethanol in DMF overnight and thoroughly washed with DMF. Palmitic acid (16 equiv, 8 per thiol group) was

[1] Abbreviations: IRRAS, infrared reflection−absorption spectroscopy; DPPC, 1,2-dipalmitoylphosphatidylcholine; DPPG, 1,2-dipalmitoylphosphatidylglycerol; π, surface pressure; *A*, molecular area; PM, polarization modulation; LE, liquid expanded; LC, liquid condensed; $\nu_a CH_2$, asymmetric methylene stretching frequency; CD, circular dichroism; NMR, nuclear magnetic resonance; HPLC, high-pressure liquid chromatography; MALDI-TOF, matrix-assisted laser desorption−ionization time-of-flight.

dissolved in methylene chloride (+ca. 1% DMF) to give a buttery foam that was reacted with the peptide resin in the presence of *O*-(benzotriazol-1-yl)-*N,N,N′-tert*-tetramethyuronium tetrafluoroborate (TBTU) (16 equiv) and diisopropylethylamine (DIEA) (32 equiv) for 4 h at 25 °C, after which an Ellman test of a resin aliquot was negative. The bis-palmitoylated peptide resin was next treated with trifluoroacetic acid (TFA)/water/triisopropylsilane (95:2.5:2.5, by volume) for 90 min, to deprotect the Arg, Asn, Lys, and Ser side chains and release the peptide from the polymer. The peptide was isolated by precipitation with chilled methyl *tert*-butyl ether, dissolved in dilute acetic acid, and lyophilized. HPLC analysis of this material on a C_4-silica column using a 40−100% linear gradient of acetonitrile (+0.036% TFA by volume) into water (+0.045% TFA by volume) over 30 min showed a main, tailing peak corresponding to ca. 75% of the area at 220 nm. The products of the synthesis were purified to >95% HPLC-homogeneus material by semipreparative HPLC on C_8-silica using a 50−80% linear gradient of acetonitrile into water (both containing 0.05% TFA by volume) over 90 min at a 3 mL/min flow rate. The purified materials had the correct amino acid analysis and gave the expected molecular mass by MALDI-TOF mass spectrometry.

Monolayer Sample Preparation, Isotherm Acquistion, and IRRAS Measurements. DPPC solutions were prepared in chloroform, and DPPG, SP-C13(palm)$_2$, SP-C13$_{L1W}$, and SP-C13$_{L1W}$(palm)$_2$ were dissolved in chloroform/methanol (3:1, v/v) at ∼1 mg/mL concentration. Lipid and peptide solutions were mixed at a 10:1 mole ratio for $\pi-A$ isotherms and IRRAS measurements.

IRRAS spectra were acquired with a Bruker Instruments Equinox 55 Spectrometer equipped with an external variable angle reflectance accessory, the XA511. The accessory is coupled to a custom-designed Langmuir trough constructed by Nima Technology Ltd. (Coventry, England) which is equipped with a Nima model PS4 surface pressure sensor. The apparatus has been described in detail previously (*24*). Briefly, the IR beam is directed through the external port in the spectrometer and is reflected by three mirrors in a rigid mount prior to being focused on the water surface. Computer-driven stepper motors rotate the mirrors to obtain the desired angle of incidence. A wire grid polarizer is placed into the optical path directly before the beam impinges on the water surface. The efficiency of polarizer, approximately 99.2%, was determined previously (*24*). The reflected light is collected at the same angle as the angle of incidence, follows an equivalent mirror path, and is directed onto a narrow band mercury cadmium telluride detector. The entire experimental setup is enclosed and purged to keep the relative humidity levels both low and as constant as feasible.

A D_2O-based subphase consisting of 150 mM NaCl and 0.1 mM EDTA in 5 mM Tris buffer at pD 6.9 was used for all experiments. A D_2O-based subphase is used to eliminate the reflectance−absorbance (RA) from the H_2O bending vibration and to lessen the absorbance from the rotation−vibration bands of water vapor, both of which occur in the conformation-sensitive Amide I region. The subphase temperature was controlled at 21.5 ± 0.5 °C. Aliquots of 5−10 μL of peptide, lipid, or lipid/peptide solution were spread dropwise on a clean surface (maximum surface area of 86 cm^2), and 1 h was allowed for solvent evaporation and film relaxation/equilibration. All samples were spread with initial surface pressures ≤7 mN/m, and $\pi-A$ isotherms were acquired during intermittent compression. The rate of compression was 0.02−0.03 nm^2/(lipid molecule·min) for all monolayers. A relaxation period of 10 min was allowed between stopping the barrier at desired surface pressure values and IRRAS spectral acquisition. IRRAS experiments were repeated a minimum of 4 times.

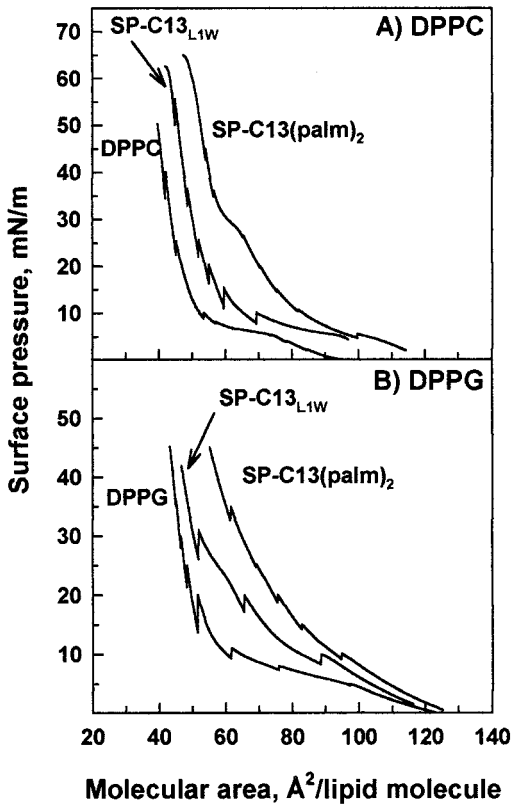

FIGURE 1: Surface pressure−molecular area ($\pi-A$) intermittent compression isotherms of DPPC (A) and DPPG (B) in the absence and presence of SP-C13(palm)$_2$ and SP-C13$_{L1W}$ at a 10:1 lipid:protein molar ratio.

Interferograms were collected with the use of a sample shuttle program to compensate for the residual water vapor rotation−vibration bands in the Amide I region. A total of 2048 scans were acquired at ∼8 cm^{-1} resolution, in 4 blocks of 512 scans each, co-added, apodized with a Blackman-Harris-3-term function, and fast Fourier transformed with one level of zero-filling to produce spectral data encoded at ∼4 cm^{-1} intervals. Spectra were acquired using p-polarized radiation at a 40° angle of incidence and s-polarized radiation at 50°.

IRRAS Data Analysis. IRRAS spectra were baseline-corrected using Grams/32 software (Galactic Industries). Peak positions and intensities were determined using a center of gravity algorithm provided by the National Research Council of Canada.

RESULTS

$\pi-A$ Isotherms. $\pi-A$ isotherms are shown in Figure 1A for DPPC in the absence and presence (10:1 lipid:protein molar ratio) of SP-C13(palm)$_2$ or SP-13C$_{L1W}$. All isotherms shown were acquired during the IRRAS experiment, i.e., in the intermittent compression mode, and display varying

decreases in pressure when the barrier is stopped. The majority of the pressure drop occurs during the relaxation period, the magnitude of the decrease dependent on the peptide and the initial pressure. The DPPC isotherm is consistent with those previously reported and exhibits the well-known liquid-expanded/liquid-condensed (LE/LC) transition at surface pressures of 5−8 mN/m (*25, 26*). The pressure drop in the mixed film of DPPC/SP-C13(palm)$_2$ was very slight (<1 mN/m) at low pressures and increased to ∼1−2 mN/m at pressures >35 mN/m, whereas a larger decrease in pressure (3−5 mN/m) was observed throughout the experiment for the nonacylated peptide.

As shown in Figure 1A, addition of the acylated peptide abolished the LE/LC transition observed for the pure lipid monolayer and revealed a reproducible kink in the isotherm at $\pi \sim 30$ mN/m. The molecular changes in the film producing this kink are revealed from the IRRAS measurements as discussed below. A kink is not observed in the isotherm of DPPC/SP-C13$_{L1W}$, and a remnant of the lipid LE/LC transition is evident. The bulk of the increase in molecular area for the peptide-containing films, compared with the pure lipid and observed at all pressures, arises from the area occupied by peptide. Peptide-induced expansion of the film is much less for the nonacylated derivative, SP-13$_{L1W}$. The isotherm in this instance is expanded by 15−25% compared to the pure lipid. This increased area is smaller than that observed for the palmitoylated peptide in which the area for a given pressure is expanded by 40−75%. These factors, along with features in the IRRAS spectra discussed below, point to a weaker interaction between the deacylated peptide and DPPC.

To explore the effect of lipid headgroup charge on the lipid/peptide interaction, $\pi-A$ isotherms are shown in Figure 1B for DPPG in the absence and presence (10:1 molar ratio) of both the deacylated and acylated peptides. The DPPG isotherm is consistent with those previously reported and exhibits a broadened LE/LC transition at 6−10 mN/m (*26*). Addition of the acylated peptide abolishes the LE/LC transition. When the deacylated peptide is mixed with DPPG, although the extent of isotherm expansion is again diminished compared to the acylated analogue, it is greater than for the DPPC/SP-C13$_{L1W}$ isotherm over a pressure range of 10−30 mN/m. This indicates that more of the deacylated peptide resides at the surface, over this π range, in the DPPG vs DPPC monolayer, most likely due to electrostatic interaction. However, as pressure is increased above 30 mN/m, the molecular area for the DPPG/SP-C13$_{L1W}$ film approaches that of the lipid alone, indicating that the depth of peptide penetration into the lipid monolayer has changed, i.e., has been reduced at $\pi > 30$ mN/m.

Peptide Effects on Lipid Conformational Order in Langmuir Films. The effect of peptide incorporation on the lipid acyl chain conformational order of DPPC in the presence of SP-C13(palm)$_2$ and SP-C13$_{L1W}$ is shown in Figure 2A. Plots of the variation in the lipid CH_2 asymmetric stretching frequency ($\nu_a CH_2$) with π for the pure lipid film reveal a rapid initial decrease from ∼2924 to ∼2920 cm^{-1} from the initial surface pressure until a pressure of ∼10 mN/m. From this point, a much smaller rate of decrease in the frequency is observed as the pressure is increased to 50 mN/m. This vibrational mode is mostly sensitive to chain conformation with a smaller contribution from chain packing (*27, 28*).

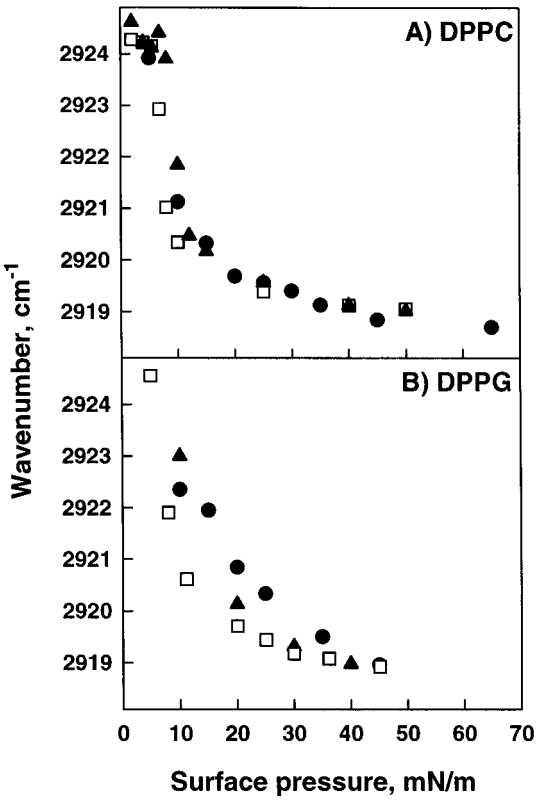

FIGURE 2: Surface pressure dependence of the CH_2 asymmetric stretching frequency of DPPC (A) and DPPG (B) in the absence (open squares) and presence of SP-C13(palm)$_2$ (filled circles) and SP-C13$_{L1W}$ (filled triangles).

Frequencies above ∼2920 cm^{-1} are indicative of chains possessing a substantial fraction of disorder, i.e., with gauche rotations in the chains. Therefore, the frequency shifts observed in the current case, at least in the initial phases of compression, arise from chain ordering [for further details about the effects of conformation versus packing changes on CH_2 stretching frequencies, see Moore et al. (*29*)]. The effect of either peptide on DPPC chain conformational ordering is small. Figure 2B displays DPPG chain ordering in the absence and presence of both peptides. In this case, the acylated peptide is shown to induce some lipid acyl chain disordering indicated by the frequency increases for pressure values up to ∼35 mN/m. The overall pressure-induced acyl chain ordering for the mixed DPPG/deacylated peptide film, however, is nearly the same as for the pure lipid monolayer.

Peptide Conformation in Langmuir Films of the Pure Peptides. Spectra of the 1500−1850 cm^{-1} region for the acylated and deacylated peptides in lipid-free Langmuir films are shown in Figure 3A−C. Isotherms acquired of the peptides during IRRAS spectral acquisition are shown as insets in the figure. The Amide I (peptide bond C═O stretch) modes of the peptides show substantial differences. The acylated species (Figure 3A,B) each show a major peak at 1635 cm^{-1} with shoulders at 1650 [SP-C13(palm)$_2$] and 1653 cm^{-1} [SP-C13$_{L1W}$(palm)$_2$]. The contour shape is relatively insensitive to surface pressure changes, although the overall intensity of the mode increases as π increases, presumably due to a greater number of molecules in the IR beam. IRRAS spectra of the control SP-C13$_{L1W}$(palm)$_2$ peptide (Figure 3B) display an Amide I contour similar to SP-C13(palm)$_2$ (Figure 3A), indicating that the L1W substitution does not signifi-

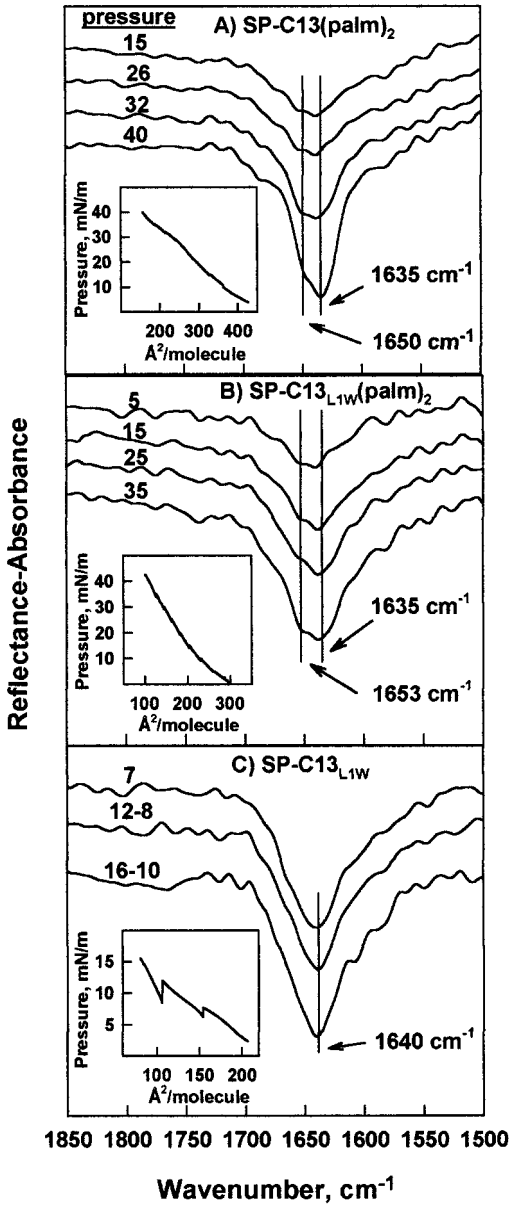

FIGURE 3: IRRAS spectra of the Amide I region for SP-C13(palm)$_2$ (A), SP-C13$_{L1W}$(palm)$_2$ (B), and SP-C13$_{L1W}$ (C) monolayers at different surface pressures. $\pi-A$ compression isotherms of the peptides are shown in the insets. Spectra were acquired using p-polarized radiation and an incident angle of 40°.

cantly affect the secondary structure of the peptide at the air/water interface. This is not surprising since the interfacial hydrophobicity values for Leu and Trp residues residing in small model peptides are similar (*30*). Differences in the isotherms of the two acylated peptides (shown as insets in Figure 3A,B) may be due to slight discrepancies in sample concentrations and/or differences in the location of specific residues with respect to the air/water interface. The deacylated peptide (Figure 3C) shows a single, relatively symmetric peak at 1640 cm^{-1}. The monolayer film of this molecule is not particularly stable, as judged by the pressure drops (noted on the inset) during the time allowed for equilibration and data acquisition, limiting the pressure range available for IRRAS measurements. This reduction in π is either due to relaxation phenomena or due to loss of peptide from the film into the aqueous subphase. Spectral assignments of the

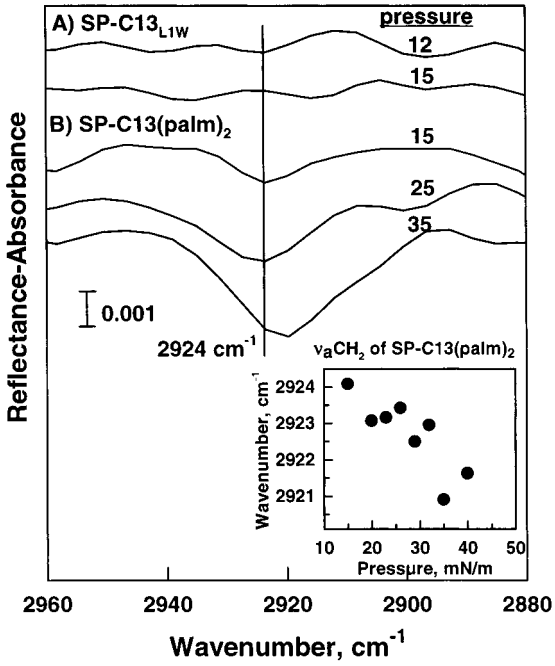

FIGURE 4: IRRAS spectra of the CH_2 asymmetric stretching region for SP-C13$_{L1W}$ (A) and SP-C13(palm)$_2$ (B) monolayers at different surface pressures. The inset shows the frequency dependence of the CH_2 asymmetric stretching vibration for SP-C13(palm)$_2$ with pressure. Spectra were acquired using p-polarized radiation and an incident angle of 40°.

Amide I contour require some explanation and are deferred to the Discussion.

The methylene stretching region (Figure 4) of the SP-C13-(palm)$_2$ peptide in a lipid-free film reveals bands from the palmitoyl chains in the peptide. As is evident from the figure, the bands are absent in the deacylated form. The frequency of the asymmetric stretching vibration for SP-C13(palm)$_2$ progressively decreases from ~2924 to ~2921 cm^{-1} as the protein film is compressed between pressures of 15 and 40 mN/m (Figure 4, inset). Despite some scatter in the data points, substantial conformational ordering is evident in the two chains upon compression of the monolayer.

Amide I Region of Lipid/SP-C13(palm)$_2$ Langmuir Films. The lipid carbonyl and protein Amide I region (1580−1780 cm^{-1}) for a 10:1 DPPC/SP-C13(palm)$_2$ film at various surface pressures is shown in Figure 5. Spectra were acquired (presented top to bottom in the figure) with increasing pressure values from 15 to 45 mN/m at intervals of 5 or 10 mN/m. From 45 mN/m, the film was reexpanded as noted to its original surface pressure. The Amide I region shows two spectral features similar to those noted in the lipid-free film (Figure 3A) appearing at ~1655 and 1639 cm^{-1}. The shape of the Amide I contour is markedly dependent on π. At π values from 15 to 30 mN/m, the former peak is the more intense. At 35 mN/m, the lower frequency component gains in intensity and becomes the stronger of the pair. The reversibility of this effect is shown by the reestablishment of the original relative intensities when the film is decompressed from 45 to 15 mN/m. The spectra in Figure 5 were acquired using p-polarized radiation which is very sensitive to changes in transition dipole orientation. To explore whether pressure-induced changes in orientation produced the intensity variation, spectra were also acquired using s-polarization which is relatively insensitive to orientation.

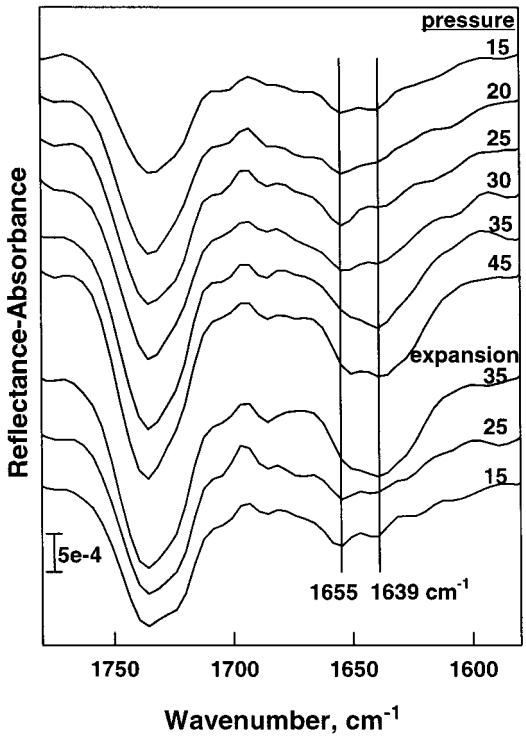

FIGURE 5: IRRAS spectra (p-polarization, 40° angle of incidence) of the lipid carbonyl and protein Amide I region (1580−1780 cm^{-1}) for a mixed film of DPPC and SP-C13(palm)$_2$ at a 10:1 lipid:peptide molar ratio. Spectra were acquired during intermittent compression (shown on top) from π = 15−45 mN/m and during expansion (shown on bottom) at the surface pressure values noted.

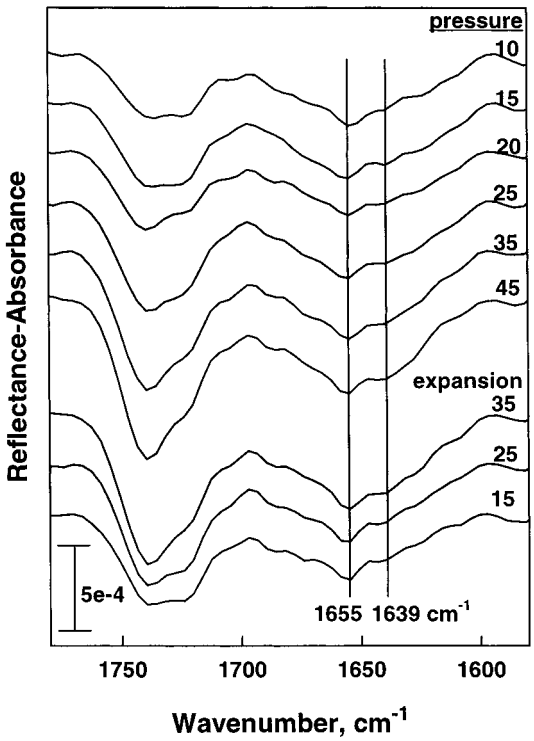

FIGURE 6: IRRAS spectra (s-polarization, 50° angle of incidence) of the lipid carbonyl and protein Amide I region (1580−1780 cm^{-1}) for a mixed film of DPPG and SP-C13(palm)$_2$ at a 10:1 lipid:peptide molar ratio. Surface pressures are noted at different points during intermittent compression and expansion.

For further details about using polarized IRRAS for orientation measurements, see the Appendix and references *24* and *31*. The relative intensities of the 1639/1655 cm^{-1} components of the Amide I contour for the DPPC/SP-C13(palm)$_2$ film are compared in Figure 7A and 7C for p- and s-polarized radiation, respectively. It is evident that similar trends are observed using both polarizations, demonstrating that the majority of the observed intensity variation is not due to pressure-induced changes in the orientation of various secondary structure elements within the peptide. This point is elaborated upon in the Appendix. In addition to the Amide I mode, subtle changes in the shape of the DPPC carbonyl stretching contour (~1735 cm^{-1}) are observed (Figure 5) which will be compared with DPPG below.

The lipid carbonyl and protein Amide I region (1580−1780 cm^{-1}) is shown as a function of π for a 10:1 (mole ratio) DPPG/SP-C13(palm)$_2$ monolayer in Figure 6. As in the DPPC/peptide films, the Amide I region again reveals two major components, at 1655 and 1639 cm^{-1}. Unlike the DPPC/SP-C13(palm)$_2$ film, the relative intensity of these two spectral features is unchanged with surface pressure, although the overall intensity of the contour is reversibly increased as π is reversibly changed between 15 and 45 mN/m. The data shown were acquired with s-polarized radiation; similar trends were observed for spectra acquired with p-polarized illumination (see Figure 7B,D). π-Dependent changes are observed in the DPPG C═O stretching modes where the two overlapped components (1740, 1725 cm^{-1}) are better resolved than in the DPPC spectra (Figure 5). The presence of two components in the carbonyl stretching mode may be attributed to subpopulations of free and hydrogen-bonded

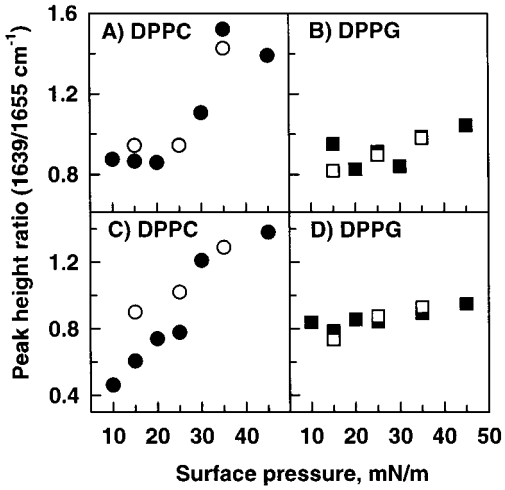

FIGURE 7: Peak height ratio of Amide I band intensities at 1639/1655 cm^{-1} as a function of surface pressure during intermittent compression (filled symbols) and expansion (open symbols) for mixed monolayers of SP-C13(palm)$_2$ with DPPC (A and C, circles) and DPPG (B and D, squares). The ratios were obtained from spectra acquired using p-polarized radiation at a 40° angle of incidence (A and B) and s-polarized radiation at a 50° angle of incidence (C and D).

carbonyl groups (*32*, *33*). At π < 25 mN/m in the DPPG mixed film (Figure 6), the lower frequency component of the overlapped doublet is relatively more intense compared to spectra acquired at π values >25 mN/m.

Amide I Region of Lipids with L1W Peptides in Langmuir Films. IRRAS spectra of DPPC and DPPG with SP-C13$_{L1W}$ are shown at surface pressures of 10, 20, 30, and 40 mN/m in Figure 8. The inset in Figure 8D overlays the two

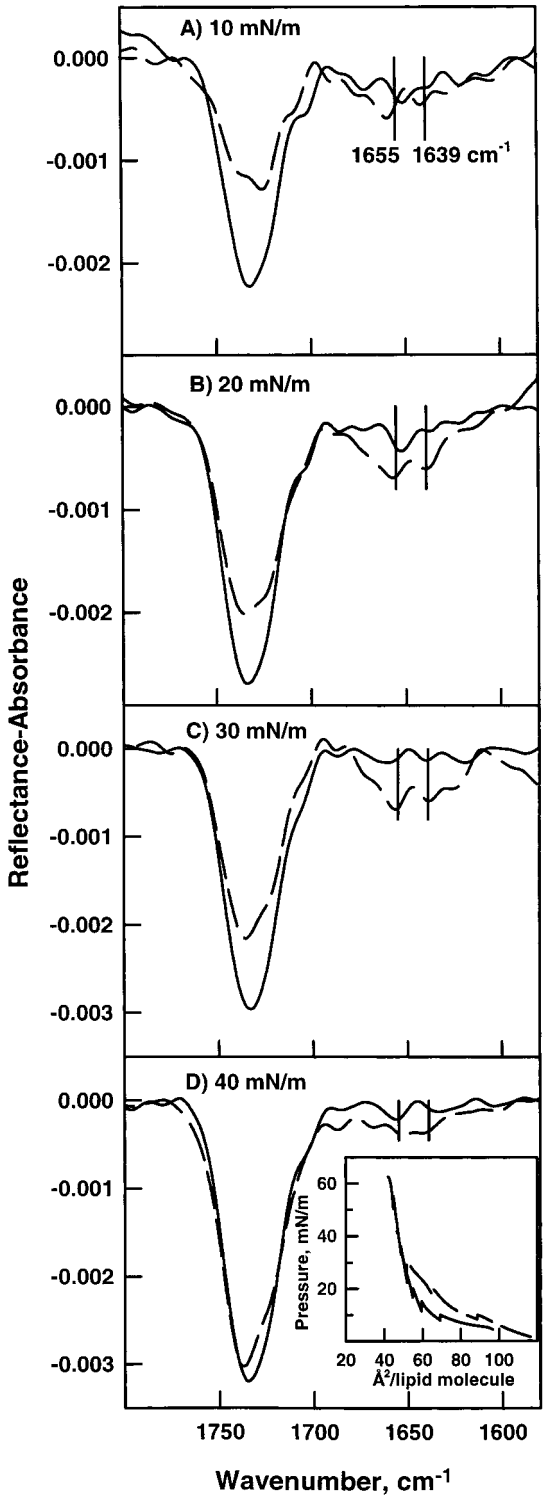

FIGURE 8: IRRAS spectra (p-polarization, 40° angle of incidence) of the lipid carbonyl and protein Amide I region (1580−1800 cm^{-1}) for a mixed film of DPPC (solid line) or DPPG (dashed line) with SP-$C13_{L1W}$ at a 10:1 lipid:peptide molar ratio at surface pressures as marked. The inset in (D) shows $\pi-A$ intermittent compression isotherms of the films.

isotherms obtained while acquiring the spectra. The intensity of the Amide I modes compared to the lipid C═O stretch is much weaker than for the mixed films of either lipid with the SP-$C13(palm)_2$ peptide (compare with Figures 5 and 6). For the DPPC/SP-$C13_{L1W}$ film, the signal levels for the peaks in the 1600−1700 cm^{-1} region are similar in intensity to the residual water vapor bands/noise (10−100 microabsorbance units) and cannot be identified with certainty at any pressure. For the DPPG/SP-$C13_{L1W}$ film, weak bands are identifiable at π values of 20 and 30 mN/m, but the Amide I intensity appears significantly reduced at 40 mN/m. This behavior is consistent with the increase in molecular area observed in the isotherm for this peptide-containing film compared to pure DPPG for intermediate π values (10−30 mN/m) and the near-merging of the DPPG/SP-$C13_{L1W}$ isotherm with that of the pure DPPG at higher pressure values (Figure 1B). Both the isotherms and the reduction of Amide I band intensity suggest loss of deacylated peptide into the subphase at higher pressures. Squeeze out of the peptide is also indicated by the merging of the two isotherms in the inset to Figure 8D (π > 30 mN/m) as the lipid carbonyl band intensities for both films approach the same value (Figure 8D). In addition, a significant change is noted in the Amide I band for the SP-$C13_{L1W}$ peptide in the presence of DPPG compared to the pure peptide film. Two components in the Amide I contour at approximately the same frequencies as for the acylated peptides are observed with DPPG compared to the fairly symmetric Amide I band centered at ∼1640 cm^{-1} for the pure SP-$C13_{L1W}$ peptide film (Figure 3C). The proximity of acyl chains, whether attached to the peptide or due to the presence of lipid, appears to perturb either the conformation or the environment of the peptide.

The lipid carbonyl and protein Amide I region for the SP-$C13_{L1W}(palm)_2$ peptide with DPPC and DPPG at various surface pressure values is shown in Figure 9. The inset shows the relative Amide I band intensities (1639/1655 cm^{-1}) as a function of pressure for the spectra acquired using s-polarized radiation. The two Amide I spectral features at ∼1655 and 1639 cm^{-1} are similar to those observed for pure SP-$C13_{L1W}(palm)_2$ films, SP-$C13(palm)_2$ monolayers in the presence and absence of lipid, and SP-$C13_{L1W}$ monolayers in the presence of DPPG only. In Figure 9, the intensity of the entire Amide I contour relative to the lipid carbonyl band for the DPPC/peptide monolayer is considerably greater than that observed for the deacylated L1W peptide (Figure 8), indicating that acylation of the peptide increases its surface activity in DPPC monolayers. As the lipid/SP-$C13_{L1W}(palm)_2$ films are compressed, an increase in the relative intensity of the low-frequency Amide I component is evident for the DPPC-containing film (Figure 9, inset), whereas the intensity distribution remains approximately the same for the DPPG/SP-$C13_{L1W}(palm)_2$ monolayer.

DISCUSSION

The current IRRAS measurements permit evaluation of the secondary structure of the N-terminal peptide of SP-C in situ at the air/water interface, and thus provide unique structural information. Interpretation of the IRRAS data for the Amide I modes requires identification of the observed peaks with particular secondary structures.

As noted above, the spectrum of SP-$C13(palm)_2$ in a pure peptide film reveals two major components in the Amide I contour, a main peak at 1635 cm^{-1} and a shoulder at 1650−1652 cm^{-1}. The assignment of the shoulder at 1650−1652 cm^{-1} to a hydrophobic α-helix is consistent with literature assignments for many hydrophobic peptides and proteins (*34*). Although the lower frequency component is more difficult to assign with certainty, several recent investigations

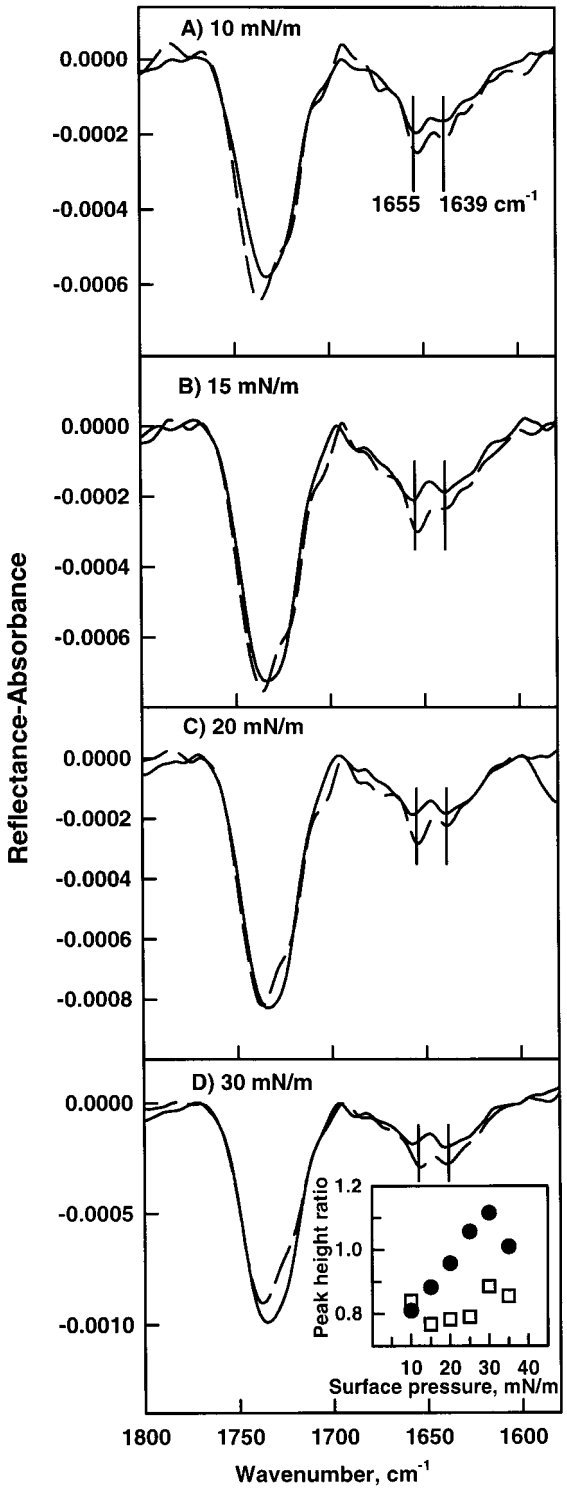

FIGURE 9: IRRAS spectra (s-polarization, 50° angle of incidence) of the lipid carbonyl and protein Amide I region (1580−1800 cm^{-1}) for a mixed film of DPPC (solid line) or DPPG (dashed line) with SP-$C13_{L1W}(palm)_2$ at a 10:1 lipid:peptide molar ratio at the surface pressure as marked. The inset in (D) shows the peak height ratio of Amide I band intensities at 1639/1655 cm^{-1} as a function of surface pressure for SP-$C13_{L1W}(palm)_2$ with DPPC (filled circles) and DPPG (open squares) during intermittent compression using s-polarized radiation at a 50° incident angle.

make a strong case that the mode be assigned to a hydrated α-helix. For example, Martinez et al. (*35*) examined the thermal unfolding of small, helical, alanine-based peptides by IR spectroscopy and observed the Amide I mode between 1632 and 1635 cm^{-1}. Williams et al. (*36*) observed a similar frequency for a small, 21 residue, alanine-based peptide.

Similar distinctions between exposed and protected Amide I modes have been proposed for globular structures. In IR studies of relaxation processes in apomyoglobin, Gilmanshin et al. (*37*) suggested the assignment of Amide I components at 1633 cm^{-1} to solvated helices and at 1650 cm^{-1} to helices protected from solvation by interhelix tertiary interactions. Along similar lines, Manas et al. (*38*) studied a synthetic α-helical coiled-coil protein, GCN4-P1′, with ^{13}C labels inserted in the amide carbonyl groups of the buried leucines or exposed alanines in separate derivatives. A shift of ∼20 cm^{-1} was observed for the Amide I peak for ^{13}C Ala amide (1585 cm^{-1}) compared with 1606 cm^{-1} for ^{13}C Leu amide. These frequency positions are of course altered from the ^{12}C isotopomers because of changes in the oscillator reduced mass, but the ∼20 cm^{-1} shift is significant for the current purposes and again reflects different α-helical Amide I frequencies for exposed vs buried environments. Thus, in a variety of synthetic and native proteins, strong evidence has recently accumulated for the assignment of spectral features between 1630 and 1640 cm^{-1} to hydrated α-helical secondary structure.

The observation of two major Amide I components in pure protein films for both acylated peptides and of a single major Amide I component in the pure SP-$C13_{L1W}$ film can be rationalized with the above assignment into a simple, coherent, and consistent structural model. The deacylated peptide forms a relatively poor Langmuir film characterized by loss of material into the subphase and concomitant drops in π during IRRAS data acquisition. As a consequence, the peptide bond C═O groups are presumably completely exposed to aqueous solvent, thereby producing an Amide I mode near 1640 cm^{-1}. In contrast, pure films of the acylated peptides (Figure 3A,B) reveal two components in the Amide I contour, reflecting the coexistence of two populations of helical peptide bonds, in accord with assignments suggested above. That is, some fraction of each acylated peptide is presumably protected from solvent interaction, possibly by the acyl chains of the S-palmitoylated Cys residues. The possible role of the acyl chains in the stabilization of the palmitoylated peptide monolayers is further indicated by the increased chain ordering shown for SP-$C13(palm)_2$ as π is increased (Figure 4). This suggests that the chains orient at the surface to stabilize the monolayer in response to increased π and also provide a hydrophobic environment for some fraction of the α-helix.

The variation in Amide I contour for the deacylated peptide in the presence and absence of lipid (DPPG) is remarkable (Figures 8 and 3C) and strengthens the helical frequency assignments established for hydrophobic/hydrophilic environments. In the presence of lipid, an additional Amide I constituent at ∼1655 cm^{-1} is observed (Figure 8C,D) and is quite similar to that of the acylated peptides in DPPG monolayers (Figures 6 and 9). Again, some fraction of the helical SP-$C13_{L1W}$ peptide bonds is apparently hydrated. The lipid acyl chains provide a hydrophobic environment for the remaining helical segments.

The Amide I contour of SP-$C13(palm)_2$ with DPPC provides unique insight into the penetration/location of the peptide in the lipid film. When the peptide interacts with DPPC, interesting changes in the relative intensities of the

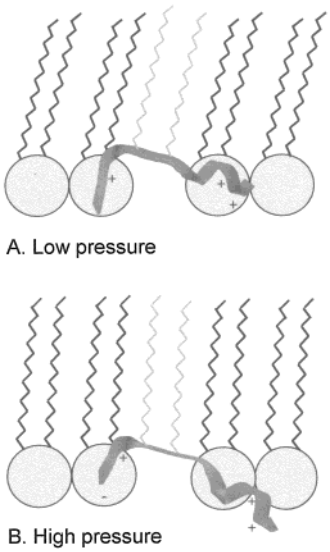

FIGURE 10: Schematic representation of the SP-C13(palm)$_2$ peptide in a lipid monolayer at low surface pressure (A) and high surface pressure (B). An unordered N-terminal region surrounding the peptide's two palmitoylcysteinyl residues (peptide acyl chains in gray), the positions of positively charged residues, and 1.5 turns of α-helix at the C-terminus are indicated. The shaded circles and black zig-zag lines represent the polar headgroups and acyl chains of the lipid, respectively. The helical portion of the peptide is inserted further within the lipid monolayer at the lower pressure and becomes more exposed to solvent at higher pressure. The peptide schematic was prepared using the program Sybyl, version 6.3.

1639−1654 cm^{-1} peak heights occur as π is increased beyond 30 mN/m (Figure 5). In pure peptide films (Figure 3A), the intensity of the low-frequency component of the contour is greater than that of the higher frequency component. This suggests that the majority of the peptide bonds are hydrated although, as noted above, a significant fraction remains in a hydrophobic environment. In films with DPPC at pressures <30 mN/m, the peak height of the 1654 cm^{-1} band (assigned to hydrophobic α-helices) is greater than the component at 1639 cm^{-1} (hydrated helices). As π is increased to 35 mN/m, the component at ∼1639 cm^{-1} gains in relative intensity, a situation which persists with further π increases. Upon reexpansion of the monolayer, the Amide I contour reverts to its initial shape. The ratio of the peak heights at 1639/1654 cm^{-1} is plotted in Figure 7. According to the interpretation given above, the proportion of hydrated helix increases at pressures ≥30 mN/m. Interestingly, this π value is close to the kink in the isotherm (Figure 1A) for this sample. The kink does not appear to reflect a change in the ordering of the lipid acyl chains as is evident in Figure 2A where the acyl chain ordering for a pure DPPC monolayer is nearly indistinguishable from the DPPC/SP-C13(palm)$_2$ film. These data, taken together, suggest that at ∼30−35 mN/m, a portion of the α-helical region of the peptide is squeezed out of the hydrophobic areas of the monolayer and thus experiences greater solvent exposure. The phenomenon is reversed upon expansion of the film due to reinsertion of the hydrated segments of the helix.

A hypothetical schematic of the acylated peptide in a DPPC monolayer under low- and high-pressure conditions is shown in Figure 10. The peptide is drawn with a disordered N-terminus and 1.5 α-helical turns at the C-terminus based on previous NMR studies of a 17 residue N-terminal SP-C peptide and native SP-C (*6*, *14*). The two palmitoyl chains of the peptide are shown inserted in the lipid monolayer. The aim of the drawing is to depict that a change in the average number of exposed residues occurs as the film is compressed. The helical region of the peptide resides in a more hydrophobic environment when the surface pressure is low (top) and experiences greater exposure to the aqueous subphase as pressure is increased (bottom). It is difficult to know whether the intensity changes in the Amide I band constituents reflect the presence of two different peptide populations on the surface where the fraction of the population shown in Figure 10A (10B) is large (small) at low π and small (large) at high π or whether each peptide molecule contains helical peptide bonds exposed to two different environments, i.e., hydrophobic and hydrophilic.

The effect of surface charge on the pressure dependence of peptide hydration is revealed in Figure 6 which presents the Amide I contour for DPPG/SP-C13(palm)$_2$ films. For this film, the ratio of the two major components of the Amide I contour is independent of π (Figure 7B,D), indicating that the helical fraction of peptide in hydrophobic vs hydrophilic environments is unchanged through the entire range of π values. This in turn indicates a stronger interaction of DPPG with the peptide compared to DPPC which may be manifest by pressure-independent penetration of the peptide in the DPPG monolayer. The stability of the peptide insertion is consistent with the absence of the kink ($\pi \sim 30$ mN/m) in the DPPG/SP-C13(palm)$_2$ vs DPPC/SP-C13(palm)$_2$ isotherm (Figures 1B and 1A, respectively). In addition, deeper insertion of the peptide into the DPPG monolayer is suggested by the increase in $\nu_a CH_2$ for this binary film which indicates that the peptide perturbs the pressure-induced lipid acyl chain ordering (Figure 2B). This is not observed for the DPPC/SP-C13(palm)$_2$ monolayer (Figure 2A). The origin of these effects presumably arises in part from the electrostatic interactions between the negatively charged headgroup of DPPG and the positively charged peptide.

Other aspects of the IRRAS spectra bear on the above discussion. The surface pressure dependencies of the lipid C═O stretching mode for both the DPPC and DPPG constituents in their respective mixed monolayer films with the SP-C13(palm)$_2$ peptide are shown in Figures 5 and 6, respectively. The C═O contour consists of two overlapped bands. After some initially contradictory interpretations of these two features in lipid spectra, definitive studies with isotopically labeled ^{13}C in single C═O groups by Blume (*32*) and subsequently by McElhaney and co-workers (*33*) have concluded that the lower frequency component (∼1720 cm^{-1}) arises from a hydrogen-bonded population of C═O groups independent of their location (*sn*-1 vs *sn*-2) in the acyl chain, while the higher frequency component (∼1740 cm^{-1}) arises from C═O groups sequestered from H-bonding possibilities, i.e., in a more hydrophobic environment. In the current studies, the relative proportions of these two populations are highly dependent upon π in the DPPG monolayer (Figure 6). As π is increased from 15 to 45 mN, the intensity of the low-frequency shoulder is diminished; the effect is reversed upon film expansion. We speculate that the interfacial region of DPPG is structured in such a way so that the hydrogen bonding of the C═O groups differs from that found in the mixed DPPC monolayers (*39*). This, along with ionic interaction, may facilitate retention of peptide in the DPPG

monolayer at the higher surface pressures, where a portion of it is squeezed out of DPPC. Bourdos et al. (*40*) have reported an enhanced interaction between SP-C and DPPG compared to DPPC in transferred Langmuir−Blodgett films. In addition, fluorescence and surface pressure investigations of the N-terminal deacylated peptide reported by Plasencia et al. (*12*) are consistent with a more stable interaction in the presence of anionic compared to zwitterionic lipids. The current results extend this observation by permitting the direct monitoring of peptide/lipid interaction in states more closely resembling physiological ones.

Finally, it is tempting to speculate on the role of S-palmitoylation in the N-terminal peptide and in native protein. The deacylated peptide, although capable of forming monolayer films with lipids, shows much weaker lipid interactions than the palmitoylated peptide, as judged both from $\pi-A$ isotherms and from the IRRAS data. The properties imparted to the N-terminal peptide through acylation appear to enhance the peptide's flexibility in interfacial environments. The native SP-C sequence is sufficiently hydrophobic so that acylation is not required to ensure its lipid interaction in Langmuir films. The role of acylation in this instance may be more subtle. As suggested by Plasencia et al. (*12*), acylation per se may be required to modulate hydrophobicity and conformation in the relatively polar N-terminal region of SP-C. Interactions between the two palmitoyl chains in the protein and lipid acyl chains in monolayer environments may permit the native peptide to remain in the vicinity of the monolayer at high surface pressures present at the end of the compression of surfactant films while the hydrophobic, helical C-terminal is bridged to nearby bilayer assemblies. In this way, acylation may aid in the transfer of SP-C and lipid from tubular myelin to the air/alveolar surface.

APPENDIX

An issue arises as to whether the relative intensity change in the Amide I components near 1635 and 1650 cm^{-1} in Figure 5 originates from changes in the proportion of the exposed and buried helical forms or from orientation changes in the helix. IRRAS spectra acquired using s- and p-polarized radiation can be used to determine the orientation of functional groups at the air/water interface (*10, 24, 31*). This determination depends on intensity variations in the reflectance−absorbance band of interest as a function of the angle of incidence and polarization state of the IR radiation. Figure 11A and 11B show the dependence of the sign, shape, and magnitude of a simulated IRRAS band in the Amide I region on helix orientation using p- and s-polarized radiation, respectively. The simulations were performed for a D_2O subphase at a 40° angle of incidence for p-polarization and at 50° for s-polarization, i.e., the same conditions as those used in the actual experiments. The equations and optical constants used in the simulation were described in reference *24*. Marked differences between the two polarizations are evident in the figure. For p-polarization, a striking change in the sign of the calculated band is observed as the helix tilt angle (angle between the helix axis and the normal to the surface) is increased from 0° to 80°. In addition, a downward shift in the frequency (~5 cm^{-1}) of the band maximum is noted. In contrast, the simulations for s-polarization show smaller intensity changes without a change in sign or frequency shift. When comparing the simulated Amide I bands to those observed experimentally, for the DPPC mixed monolayer acquired using p-polarized radiation (Figure 5), the shape and sign of the experimental Amide I band components unequivocally demonstrate that the helix tilt angle must be greater than ~30° for the measured surface pressure values. For tilt angle changes in the 40−80° range, the simulations show a much greater intensity variation for p-polarized compared to s-polarized radiation. This is not observed in the experimental spectra, which are essentially the same for the two polarizations. Although minor helix tilt angle changes in the 40−80° range may account for a small degree of the experimentally observed intensity variation, the observed frequencies of the component bands and the majority of the intensity variation are consistent with alteration in helix hydration rather than a change in the orientation of the helix.

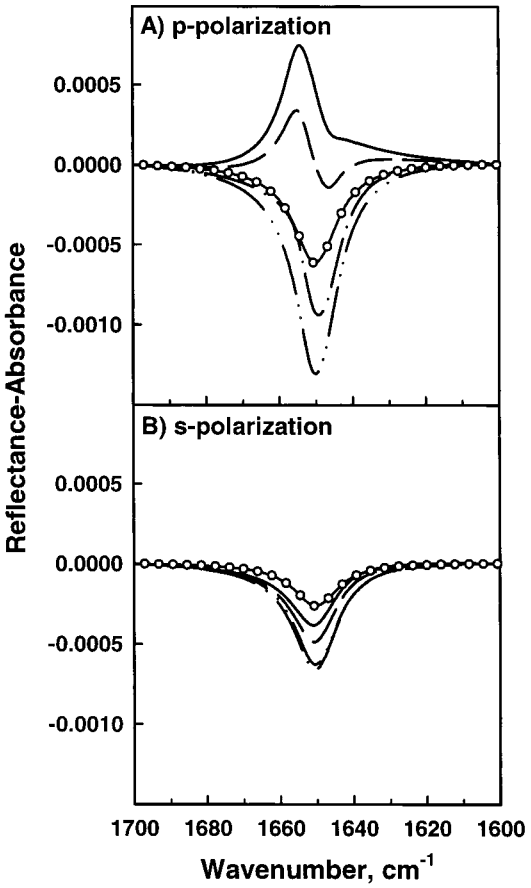

FIGURE 11: Simulations of the effect of changed helix orientation on the Amide I mode spectral parameters. The helix is assumed to be in a monolayer on a D_2O subphase. The initial frequency of the Amide I band is 1650 cm^{-1} with the Amide I transition moment assumed to lie 28° from the helix axis. See reference *24* for optical constants used in the simulations. The Amide I band was simulated at the following helix tilt angles: 0° (solid line); 20° (dashed line); 40° (dashed−dotted line); 60° (dashed−dotted−dotted line); 80° (solid−open circle line) in (A) for p-polarized radiation and (B) s-polarized radiation.

REFERENCES

1. Johansson, J., and Curstedt, T. (1997) *Eur. J. Biochem. 244*, 675−693.
2. Goerke, J. (1998) *Biochim. Biophys. Acta 1408*, 79−89.
3. Veldhuizen, E. J. A., and Haagsman, H. P. (2000) *Biochim. Biophys. Acta 1467*, 255−270.

4. Walther, F. J., Gordon, L. M., Zasadzinski, J. A., Sherman, M. A., and Waring, A. J. (2000) *Mol. Genet. Metab. 71*, 342−351.
5. Johansson, J., Curstedt, T., and Robertson, B. (2001) *Pediatr. Pathol. Mol. M. 20*, 501−518.
6. Johansson, J., Szyperski, T., Curstedt, T., and Wuthrich, K. (1994) *Biochemistry 33*, 6015−6023.
7. Creuwels, L., Demel, R. A., Vangolde, L. M. G., Benson, B. J., and Haagsman, H. P. (1993) *J. Biol. Chem. 268*, 26752−26758.
8. Wang, Z. D., Gurel, O., Baatz, J. E., and Notter, R. H. (1996) *J. Biol. Chem. 271*, 19104−19109.
9. Flach, C. R., Gericke, A., Keough, K. M. W., and Mendelsohn, R. (1999) *Biochim. Biophys. Acta 1416*, 11−20.
10. Gericke, A., Flach, C. R., and Mendelsohn, R. (1997) *Biophys. J. 73*, 492−499.
11. Johansson, J., Nilsson, G., Stromberg, R., Robertson, B., Jornvall, H., and Curstedt, T. (1995) *Biochem. J. 307*, 535−541.
12. Plasencia, I., Cruz, A., Casals, C., and Pérez-Gil, J. (2001) *Biochem. J. 359*, 651−659.
13. Plasencia, I., Rivas, L., Casals, C., Keough, K. M. W., and Pérez-Gil, J. (2001) *Comp. Biochem. Physiol., A 129*, 129−139.
14. Johansson, J., Szyperski, T., and Wuthrich, K. (1995) *FEBS Lett. 362*, 261−265.
15. Yousefi-Salakdeh, E., Johansson, J., and Strömberg, R. (1999) *Biochem. J. 343*, 557−562.
16. Dluhy, R. A., and Cornell, D. G. (1985) *J. Phys. Chem. 89*, 3195−3197.
17. Dluhy, R. A. (1986) *J. Phys. Chem. 90*, 1373−1379.
18. Flach, C. R., Brauner, J. W., Taylor, J. W., Baldwin, R. C., and Mendelsohn, R. (1994) *Biophys. J. 67*, 402−410.
19. Blaudez, D., Buffeteau, T., Cornut, J. C., Desbat, B., Escafre, N., Pezolet, M., and Turlet, J. M. (1994) *Thin Solid Films 242*, 146−150.
20. Merrifield, B. (1986) *Science 232*, 341−347.
21. Andreu, D., Ubach, J., Boman, A., Wahlin, B., Wade, D., Merrifield, R. B., and Boman, H. G. (1992) *FEBS Lett. 296*, 190−194.
22. Beekman, N. J., Schaaper, W. M. M., Tesser, G. I., Dalsgard, K., Kamstrup, S., Langeveld, J. P., Boshuizen, R. S., and Meloen, R. H. (1997) *J. Pept. Res. 50*, 357−364.
23. Barany, G., Albericio, F., Solé, N. A., Griffin, G. W., Kates, S. A., and Hudson, D. (1993) in *Proceedings of the Twenty-second European Peptide Symposium* (Schneider, C. H., and Eberle, A. N., Eds.) pp 267−268, ESCOM, Leiden.
24. Flach, C. R., Xu, Z., Bi, X., Brauner, J. W., and Mendelsohn, R. (2001) *Appl. Spectrosc. 55*, 1060−1066.
25. Phillips, M. C., and Chapman, D. (1968) *Biochim. Biophys. Acta 163*, 301−313.
26. Rana, F. R., Mautone, A. J., and Dluhy, R. A. (1993) *Biochemistry 32*, 3169−3177.
27. Snyder, R. G., Strauss, H. L., and Elliger, C. A. (1982) *J. Phys. Chem. 86*, 5145−5150.
28. MacPhail, R. A., Strauss, H. L., Snyder, R. G., and Elliger, C. A. (1984) *J. Phys. Chem. 88*, 334−341.
29. Moore, D. J., Rerek, M. E., and Mendelsohn, R. (1997) *J. Phys. Chem. B 101*, 8933−8940.
30. Wimley, W. C., and White, S. H. (1996) *Nat. Struct. Biol. 3*, 842−848.
31. Flach, C. R., Gericke, A., and Mendelsohn, R. (1997) *J. Phys. Chem. B 101*, 58−65.
32. Blume, A., Hübner, W., and Messner, G. (1988) *Biochemistry 27*, 8239−8249.
33. Lewis, R. N. A. H., McElhaney, R. N., Pohle, W., and Mantsch, H. H. (1994) *Biophys. J. 67*, 2367−2375.
34. Haris, P. I., and Chapman, D. (1996) in *Infrared Spectroscopy of Biomolecules* (Mantsch, H. H., and Chapman, D., Eds.) pp 239−278, Wiley-Liss, Inc., New York.
35. Martinez, G., and Millhauser, G. (1995) *J. Struct. Biol. 114*, 23−27.
36. Williams, S., Causgrove, T. P., Gilmanshin, R., Fang, K. S., Callender, R. H., Woodruff, W. H., and Dyer, R. B. (1996) *Biochemistry 35*, 691−697.
37. Gilmanshin, R., Williams, S., Callender, R. H., Woodruff, W. H., and Dyer, R. B. (1997) *Proc. Natl. Acad. Sci. U.S.A. 94*, 3709−3713.
38. Manas, E. S., Getahun, Z., Wright, W. W., DeGrado, W. F., and Vanderkooi, J. M. (2000) *J. Am. Chem. Soc. 122*, 9883−9890.
39. Zhang, Y.-P., Lewis, R. N. A. H., and McElhaney, R. N. (1997) *Biophys. J. 72*, 779−793.
40. Bourdos, N., Kollmer, F., Benninghoven, A., Ross, M., Siever, M., and Galla, H.-J. (2000) *Biophys. J. 79*, 357−369.

BI020129G